Construction of donor-acceptor type conjugated microporous polymers: A fascinating strategy for the development of efficient heterogeneous photocatalysts in organic synthesis

Yongfeng Zhi[a], Si Ma[a], Hong Xia[b],*, Yumin Zhang[a], Zhan Shi[c], Ying Mu[a], Xiaoming Liu[a],*

[a] State Key Laboratory for Supramolecular Structure and Materials, College of Chemistry, Jilin University, Changchun, 130012, PR China
[b] State Key Laboratory on Integrated Optoelectronics, College of Electronic Science and Technology, Jilin University, Changchun, 130012, PR China
[c] State Key Laboratory of Inorganic Synthesis and Preparative Chemistry, College of Chemistry, Jilin University, Changchun, 130012, PR China

ARTICLE INFO

ABSTRACT

Metal-free, visible-light driven, solid organic photocatalysts provide a more green and environmentally friendly alternative to traditional metal-based photocatalysts. Donor-Acceepor (D-A) dyads possess a feature of easy to adjust the photoelectric properties, and enhance their photocatalytic performances. Here we report a fascinating strategy for screening excellent organic porous photocatalysts through oxidative coupling of single D-A based monomer, which has still an important advantage to ensure uniformity of polymer structure except for the inherent characteristics of D-A polymers. According to this strategy, three D-A typed conjugated microporous polymer (DA-CMP) photocatalysts consisting of alternating electron-rich (carbazole) and electron-deficient (benzene, 4,7-diphenyl-2,1,3-benzothiadiazole or anthraquinone) units have been synthesized, and their porosity and photoelectric properties including adsorption, emission, lifetime, optical bandgaps, energy levels and transient photocurrent response as well as photocatalytic activity, were conveniently tuned by selecting different D-A monomers with tunable electron-deficient moiety. These DA-CMPs were exploited as metal-free photocatalysts in the oxidative C-H functionalization reactions in the presence of visible-light and molecular oxygen. They showed excellent photocatalytic activity, extensive substrate adaptability and outstanding reusability, due to combining some key features like permanent porosity, outstanding stability and optoelectronic properties. In addition, the reaction mechanism for DA-CMP photocatalyzed C-H functionalization reactions under visible-light irradiation was investigated in detail. Moreover, to prove in depth the benefits of the heterogeneous photocatalysis, a continuous flow procedure has been conducted with an excellent yield.

1. Introduction

Over the last decade, light-driven organic transformation has attracted much attention due to its high selective, mild reaction condition and environmentally friendly process [1–4]. Because of their excellent absorptive capacity for visible-light and rich redox potentials in the excited state, organometallic compounds based on precious transition metals like ruthenium or iridium [5–10] and pure molecule-based organic dyes [11,12] have been widely employed as photocatalysts for many important organic reactions. However, some intrisic drawbacks of these homogeneous catalytic systems such as high price and toxicity of rare metals, the depressing stability of the organic dayes, low recyclability and tedious product purification steps for catalyst separation, which hinder their practical applications in scale-up preparation of the fine chemicals [13–15]. Recent exploration on the hybrid porous

materials including metal-organic frameworks, transition-metal complexes doping porous polymers only partially alleviates the issue of reusability [16–19]. From a standpoint of sustainable application, therefore, the constrution of efficient solid photocatalysts that combine the requirements of low cost, outstanding catalytic activity and excellent reusbility is also an urgent desire.

Since the pioneering research on g-C$_3$N$_4$ as photocatalyst in 2009 [20], the metal-free semiconductor-based heterogeneous photocatalysts have attracted tremendous scientific attentions, because they can prove a more sustainable and environmetally benign choice. In particular, exporation of conjugated microporous polymers (CMPs) as a new kind of ideal heterogeneous photocatalytic platform has recently emerged, which is attributed to their large specific surface area, permanent nanopores, good absorption in the visible region and outstanding stability, as well as chemical tailor of conjugated skeletons [21–23]. Previous

research results have proven the potential applications of CMPs in light-induced hydrogen evolution [24–28], selection oxidation of sulfides [29–31], molecular oxygen activation [32–34], photocatalytic oxidative coupling of amines [35–37], oxidative carbon-hydrogen functionalizations [38–40] and so on [41–44]. Unfortunately, most of these three-dimensional conjugated polymer materials as solid photocatalysts bear a relatively low specific surface area and noble metal catalyst for their synthesis [24,36,37]. Currently, CMPs based photocatalysts combining low-cost of synthesis, high catalytic efficiency and excellent recyclability have been rare. The strategy to accurately tailoring the optical and electronic properties of CMPs for enhancing the photocatalytic efficiency has not been reported.

Carbazole-containing π-conjugated systems possess intriguing photoelectric performance, and are widely utilized as electronic transmission and emission materials in organic light-emitting diodes and photovoltaic devices [45,46]. And it has still been demonstrated that carbozle-based compounds are easily converted into porous organic networks through oxidative coupling polymerization [47–51]. Therefore, we envisioned that the predesigned carbozle-based CMPs with the electronic donor-acceptor (D-A) properties could serve as efficient, cheap, heterogeneous photocatalyst for organic reactions. First, the carbazole derivatives are easily prepared through commercial materials, and allow scale-up synthesis. Second, the polymerization pathway of oxidative coupling by FeCl₃ can effectively reduce the cost of porous polymers. Third, the rigid backbone of carbazole derivatives is favorable for the consturction of a metal-free porous network with permanent porosity and excellent stability. Fourth, by changing the electronic features of linker in carbozle-based monomer is easy to implement the precise tailoring of photo/electronic characteristics of conjugated polymer networks. More importantly, it is easy to screen out excellent CMPs based photocatalysts from a series of tunable D-A typed polymers. Herein, we report a fascinating strategy for screening excellent organic porous photocatalysts through oxidative coupling of single carbazole based monomer with electronic D-A properties, which has still an important advantage to ensure uniformity of polymer structure except for the inherent characteristics of D-A type polymers. Along this line, three carbazole-based DA-CMPs have been designed and constructed, and their color, porosity and photoelectric properties were conveniently tuned by selecting different DA monomer. Importantly, the DA-CMPs were found to be metal-free heterogeneous photocatalysts with great catalytic activity, extensive substrate adaptability and outstanding reusability in the oxidative C-H functionalizations of N-aryltetradroisoquinolines under visible-light irradiation and molecular oxygen as green oxygen source. And their photocatalytic performances surpass that of the crystalline covalent organic framework material reported by our group [44]. The responsible mechanism for DA-CMPs for the organic transformation was also full investigated.

2. Experimental

2.1. Chemical and materials

The 1,4-Dimethoxybenzene, bromine, 4-aminobenzonitrile were obtained from Sinopharm Chemical Reagent. Trifluoromethanesulfonic acid and n-Butyllithium solution in hexanes (1.6 M) were obtained from J&K Scientific. Other organic solvents for reactions were distilled over appropriate drying reagents under nitrogen. Deuterated solvents for NMR measurement were obtained from Aladdin. 4,4`-biscarbazolylbenzene, 4,7-di[4-(carbazol-9-yl)phenyl]benzo [1,2,5]thiadiazole, 2,6-di(9H-carbazol-9-yl)anthracene-9,10-dione were synthesized according to the reported methods [52–54].

2.2. Synthesis of the polymers

Three carbozle-based conjugated microporous polymers (DA-CMPs) were synthesized via FeCl₃-catalyzed oxidative coupling reaction using
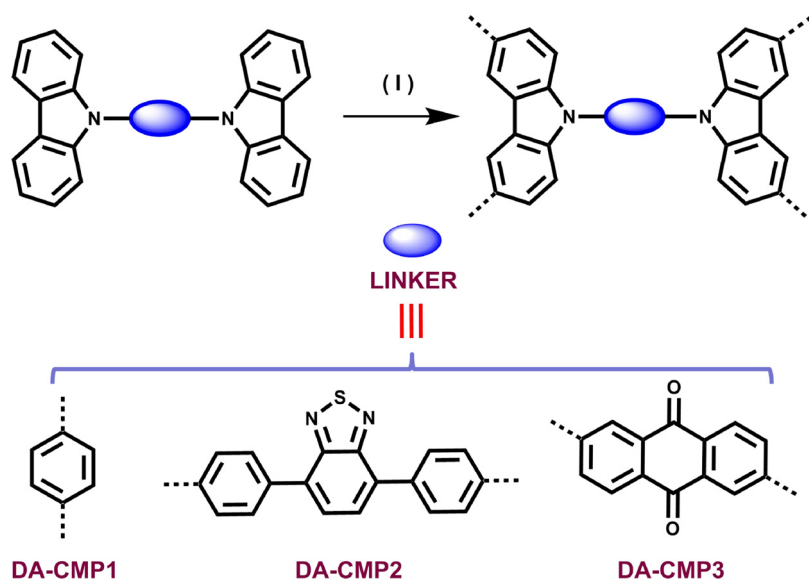
D-A typed carbazole compounds as a single monomer. The DA monomer 3 (150 mg, 0.279 mmol) was dispersed in anhydrous chloroform (30 mL), and then transferred dropwise to a suspension of ferric chloride (453 mg, 2.79 mmol) in anhydrous chloroform (15 mL). The mixture was stirred for 2 days under nitrogen at 60 °C, and then 50 mL of methanol was added to the reaction mixture. The resulting mixture was kept stirring for another hour and the precipitate was collected by filtration and washed with methanol, dichloromethane and acetone, respectively. The powder was vigorously treated with aqueous hydrochloric acid 37% for 2 h, filtered and washed with water and methanol, dichloromethane and acetone, respectively. The further purification of the network was extracted using a Soxhlet extractor with methanol and THF for 24 h. The target product was dried at 120 °C under vacuum for 24 h to give a red powder (yield: 95%). Elemental combustion analysis (%) Calcd for $(C_{38}H_{18}N_2O_2)_n$: C, 85.38%; H, 3.39%; N, 5.24%; Found C, 79.39%; H, 2.95%; N, 4.34%. The detail of the synthesis for the other polymers is given in the Supporting Information.

2.3. Characterization

The infrared spectra were recorded from 400 to 4000 cm⁻¹ on an Avatar FT-IR 360 spectrometer by using KBr pellets. ¹H spectra were recorded on a Avance III-400 NMR spectrometer, where chemical shifts (δ in ppm) were determined with a residual proton of the solvent as standard. Solid-state ¹³C CP/MAS NMR measurement was recorded using a Bruker AVANCE III 400 WB spectrometer at a MAS rate of 5 kHz and a CP contact time of 2 ms. Elemental analyses were carried out on an Elementar model vario EL cube analyzer. UV/Vis spectra have been carried out on a Perkin Elmer Lambda 950 spectrophotometer within the wavelength range 200–700 nm. Field emission scanning electron microscopy was performed on a SU8020 model HITACHI microscope. Transmission electron microscopy was performed on a JEOL model JEM-2100 microscope. The sample was prepared by drop-casting a supersonicated methanol suspension of polymer onto a copper grid. Powder X-ray diffraction data were recorded on a PANalytical BV Empyrean diffractometer diffractometer by depositing powder on glass substrate, from $2\theta = 1.5°$ to 45° with 0.02° increment at 25 °C. Thermogravimetric analysis (TGA) was performed on a TA Q500 thermogravimeter by measuring the weight loss while heating at a rate of 10 °C min⁻¹ from room temperature to 800 °C under nitrogen. Nitrogen sorption isotherms were measured at 77 K with a JW-BK 132 F analyzer. Before measurement, the samples were degassed in vacuum at 120 °C for more than 10 h. The Brunauer-Emmett-Teller (BET) method was utilized to calculate the specific surface areas and pore volume. The nonlocal density functional theory (NLDFT) method was applied for the estimation of pore size distribution. Absolute fluorescence quantum yields were measured on an Edinburgh FLS920 steady state spectrometer using an integrating sphere. Luminescence decay experiments were carried out on an Edinburgh FLS920 spectrometer. The EPR spectra were recorded on a JEOL JES-FA200 EPR spectrometer. Samples were quantitatively injected into specially made quartz capillaries for ESR analysis. The date of DMPO and TEMP solution with the concentration of 0.1 M were collected under this instrument parameters: scanning frequency, 9.05 GHz; central field, 323 m T; scanning width, 100 G; scanning power, 5 mW; scanning temperature: 293 K. All the irradiations were performed with > 400 nm continuous laser.

2.4. Electrochemical measurements

Electrochemical measurements were performed in a three-electrode system with a VersaSTAT 3 electrochemical workstation (AMETEK Scientific Instruments, USA). The glass carbon electrode (GCE) was used as working electrode, a platinum wire electrode, and a saturated calomel electrode (SCE) as counter and reference electrode, respectively. To create measurable polymer films, the polymer was mixed and ground with 5 wt % Nafion, the mixture was dropped on top of a glassy

Scheme 1. Synthetic procedure to DA-CMPs by oxidative coupling polymerization reaction (I) $FeCl_3$/$CHCl_3$.

carbon working electrode, and the solvents were evaporated in a vacuum oven for at least 30 min. The measurements were carried out in a 0.1 M solution of tetrabutylammonium hexafluorophosphate in acetonitrile. A Pt counter electrode and a SCE reference electrode were used. Scan rate: 100 mV/s, T = 25 °C. The photocurrent of the polymer was measured on VersaSTAT 3 electrochemical workstation under UV–vis light irradiation with 25 s light on-off cycles. The working electrode prepared from the polymer catalyst and 5 wt% Nafion was immersed in 0.1 M Na_2SO_4 aqueous solution.

2.5. A general procedure for the aerobic CDC reaction of tetrahydroisoquinolines

Tetrahydroisoquinoline derivatives (0.1 mmol), nitromethane (1.0 mmol), DA-CMP3 (2.0 mg) and methanol (1.0 mL) were mixed in a 10-mL reaction tube with magnetic stirring bar. The mixture was bubbled with a stream of oxygen for 30 min. The tube was then sealed and irradiated with a blue LED lamp for 1 h at 25 °C. Thin layer chromatography (TLC) was used to monitor the progress of the reaction. After the completion of the reaction, the solvent was evaporated under reduced pressure. The residue was subjected to ^{1}H-NMR spectroscopic analysis and purified by column chromatography on silica gel using petroleum ether/ethyl acetate (10:1) as eluent. The detail of other Photocatalytic is given in the Supporting Information.

2.6. A general procedure for the alkynylation coupled with photoredox catalysis [55]

Tetrahydroisoquinoline derivatives (0.2 mmol), DA-CMP3 (4.0 mg) and methanol (2.0 mL) were mixed in a 10 mL reaction tube with magnetic stirring bar. The mixture was bubbled with a stream of oxygen for 30 min. The tube was then sealed and irradiated with a blue LED lamp for 1 h at 25 °C. Thin layer chromatography (TLC) was used to monitor the progress of the reaction. After the starting material was consumed as indicated by TLC, the blue LED lamp was removed and the reaction vessel was covered with aluminum foil before Et_3N (138.6 μL, 1 mmol, 5.0 equiv), CuBr (4.3 mg, 0.03 mmol, 0.15 equiv), and phenylacetylene (109.8 μL, 1.0 mmol, 5.0 equiv) were added successively. Then stirred at room temperature for 12 h, the reaction was filtered and concentrated the crude oil was purified via silica gel chromatography (petroleum ether/ethyl acetate 60:1) to afford the desired product.

2.7. Recycle experiments for the aerobic CDC reaction of 2-phenyl-1,2,3,4-tetrahydroisoquinoline with nitromethane

2-phenyl-1,2,3,4-tetrahydroisoquinoline (0.5 mmol), nitromethane (5.0 mmol), DA-CMP3 (10.0 mg) and methanol (5.0 mL) were mixed in a 10 mL reaction tube with magnetic stirring bar. The mixture was bubbled with a stream of oxygen for 30 min. The tube was then sealed and irradiated with a blue LED lamp at 25 °C. After the first run reaction was finished, the photocatalyst DA-CMP3 was recovered by centrifugation, and then washed thoroughly with THF and CH_2Cl_2 to remove any residual products or unreacted substrates. The recovered DA-CMP3 was dried under vacuum at 100 °C overnight. The used photocatalyst DA-CMP3 was re-employed in next cycle under identical conditions.

2.8. Continuous flow system

The system consists of a transparent glass column (r = 0.35 cm, L = 5.0 cm) end-capped with two frits, equipped with FEP-tubing and charged with 5.0 mg of DA-CMP3. T-part fitting was used to mix the solution of 2-phenyl-1,2,3,4-tetrahydroisoquinoline (0.1 M in methanol) and CH_3NO_2 (6.0 mmol, 0.32 mL) which was delivered by a syringe pump, with oxygen gas (5.0 mL min^{-1}). The reaction mixture was pumped through the microreactor with the desired flow rate (150 μL min^{-1}). The transparent glass column was irradiated with the blue light LED lamp (460 nm, 30 W) and was mounted in a 2.0 cm distance from the vial. The crude product was collected at the end of the reactor and then were taken directly from the output and the conversion was determined by ^{1}H NMR, the yield was 99.9%.

3. Results and discussion

Three carbozle-based conjugated microporous polymers (DA-CMPs) were synthesized via $FeCl_3$-catalyzed oxidative coupling reaction using D-A typed carbazole compounds as a single monomer (Scheme 1). The optical and electronic properties of these conjugated homopolymers are not only easy to be adjusted by changing the linker, but also their stucture repeatability is better than that of copolymer networks. Note that a known polymer DA-CMP1 was synthesized as a comparision to research the structural effect on photoelectronic and photocatalytic performances [52]. Three polymer networks are insoluble in water and all common organic solvents tested such as alcohol, dichloromethane, trichloromethane, toluene, tetrahydrofuran (THF), acetone and N,N`-

dimethylformamide (DMF). In addition, they are still chemical stable for dilute solution of acid and base. Compared with the corresponding monomer, the FT-IR spectrum of DA-CMPs retains some characteristic peaks in the some positions, but more broadening profiles according with the features of the networks (Fig. S1 in the Supporting Information). The atomic-level structure of DA-CMPs was assessed by solid state ^{13}C NMR (Fig. S2). The ^{13}C CP/MAS NMR spectra of DA-CMP2 exhibit five broad signals at 109, 119, 125, 137 and 153 ppm, respectively. The peak at 109 ppm can be attributed to the unsubstituted aryl carbons next to the nitrogen atom in carbazole building-units. The low-field signal at 153 ppm correspond to the carbon atom of the C=N structure and other peaks assigned to the substituted and unsubstituted aryl carbon in the polymer backbone. However, the characteristic signal of C=O group for DA-CMP3 appeared in the lower field at about 180 ppm. Thermogravimetric analysis (TGA) indicates that the DA-CMPs possess an outstanding thermal stability, which corresponds to a significant decomposition temperature above 500 °C (Fig. S3). Powder X-ray diffraction (PXRD) profiles did not show any peaks, indicating that DA-CMPs have an amorphous structure (Fig. S4). Field-emission scanning electron microscopy (FE-SEM) images show that the DA-CMP3 adopts a sphere-like morphology with a size of 50–100 nm. For DA-CMP1 and DA-CMP2, however, the images displayed that both solid samples are composed of banded particles at the micrometer scale (Fig. S5).

The permanent porosity of DA-CMPs was characterized by nitrogen adsorption-desorption measurements at 77 K. As shown in Fig. 1a, DA-CMPs display a combination of type I and type II nitrogen sorption isotherms features, according to the IUPAC classification. The obtained curves show a steep adsorption of N_2 at low relative pressure of $p/p_0 < 0.05$ and the gradual increase in the N_2 uptake with increasing pressure, reflecting the co-existence both micropores and mesopore in the DA-CMPs. Derived from the N_2 adsorption data, the Brunauer-Emmett-Teller (BET) surface area and total volume of DA-CMP1 were evaluated to be 1032 $m^2 g^{-1}$ and 0.915 $cm^3 g^{-1}$, which was higher than the previous reports [52]. Because of the strong π-π stacking interaction between the linkers [56], two other polymers exhibited a lower specific surface area of 617 $m^2 g^{-1}$ for DA-CMP2 and 758 $m^2 g^{-1}$ for DA-CMP3, respectively. The corresponding total volume of both polymers were
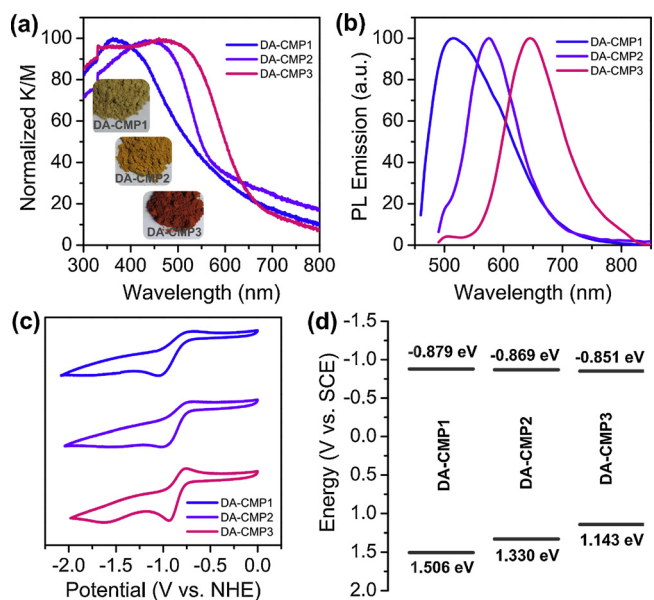
Fig. 2. (a) Normalized absorption spectra and photographs (inset) of DA-CMPs. (b) Photoluminescence spectra of DA-CMPs measured in the solid state. (c) Solid-state cyclic voltammetry of DA-CMPs with a scan rate of 100 mV s^{-1}. (d) HOMO and LUMO band position of DA-CMPs.

still calculated to be 0.503 and 0.601 $cm^3 g^{-1}$ at $p/p_0 = 0.99$. Based upon the evaluations of the Saito-Flory method, the pore sizes of the DA-CMPs are distributed around 0.6 ~ 1.7 nm and 2.0 ~ 3.1 nm, respectively (Fig. 1b). In additoin, the high-resolution transmission electron microscopy (HR-TEM) images further revealed the existence of hierarchical porosities for all DA-CMPs (Fig. 1c–e). The hierarchical porous structure of DA-CMPs is very beneficial for the diffusion and transformation of matters in the photocatalytic reactions [57].

The effect of the linker on the photophysical properties of the obtained DA-CMPs was investigated by UV–vis diffuse reflectance
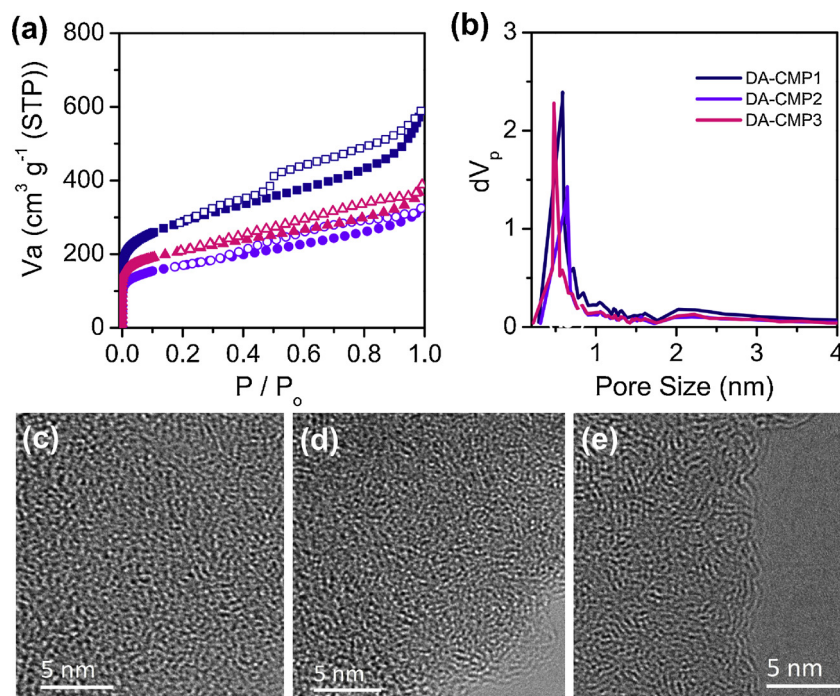
Fig. 1. (a) Nitrogen adsorption (full) and desorption (empty) isotherm of DA-CMP1 (circle), DA-CMP2 (triangle) and DA-CMP3 (square) at 77 K. (b) Pore size distribution of DA-CMPs on the N_2 adsorption isotherm. HR-TEM images of DA-CMP1 (c), DA-CMP2 (d), and DA-CMP3 (e).

spectroscopy. As shown in Fig. 2a, all DA-CMPs in the solid state showed broad absorption bands with a range from the ultraviolet to visible light regions. The DA-CMP1 has an absorption maximum at 370 nm, and a distinct red-shift of the absorption peaks is observed for two other DA-CMPs with a stronger electron-deficient linker. The spectrum of DA-CMP2 and DA-CMP3 demonstrated an absorption maximum at 445 and 482 nm, respectively. This still corresponds to the color change in the DA-CMPs, from yellowish for DA-CMP1, orange for DA-CMP2 to brown for DA-CMP3 (Fig. 2a, inset). Upon excitation at the corresponding absorption peak, the solid samples of DA-CMPs showed a luminescence band with a maximum peak centred at 514 nm for DA-CMP1, 576 nm for DA-CMP2 and 645 nm for DA-CMP3, respectively (Fig. 2b). The optical band gap of DA-CMP1, DA-CMP2 and DA-CMP3 were determined to be 2.385, 2.199 and 1.994 eV, respectively, which was evaluated via Kubelka-Munk function (Fig. S6). To further investigate the electronic structures of DA-CMPs, cyclic voltammetry (CV) measurements were performed. The CV profiles displayed the semi-reversible reductive peaks with the reductive potential ($E_{1/2}^{red}$) gradually decreases from −0.879 eV (DA-CMP1) to −0.851 eV (DA-CMP3) (Fig. 2c). The valence band (VB) position at 1.506 eV for DA-CMP1, 1.330 eV for DA-CMP2, and 1.143 eV for DA-CMP3 could be thus derived from the optical band gap (Fig. 2d). These data are comparable to the redox potentials of classical transition metal complexes [5–10].

The aerobic cross dehydrogenative coupling (CDC) reaction [58–60] offers an elegent pathway for the efficient construction of new carbon-carbon and carbon-heteroatom bonds. Among them, particularly, the visible-light photocatlytic carbon-hydrogen functionalization of tertiary amines is a most atom-economic and sustainable reaction process. Therefore, we evaluated and compared the photocatalytic performances of DA-CMPs in carbon-hydrogen functionalization of N-aryltetrahydroisoquinonlines with vairous nucleophiles under irradiation of visible-light at 25 °C in the presence of O_2 as oxygen source. The aerobic CDC reaction of N-phenyl-1,2,3,4-tetrahydroisoquinoline **1a** with nitromethane **2a** containing a catalytic amount of DA-CMP3 was selected as model photocatalytic reaction to optimize reaction conditions. The effect of different solvents, the rate of both reactants and light source on the yield was first investigated. As can be seen Table S1, toluene, dioxane, acetonitrile, DMF, and THF as the solvent, low yields were obtained (5–19%, Table S1, entries 1–5). Then the reaction was performed in ethanol and the moderate yield was shown (46%, Table S1, entry 6). Compared with ethanol, however, an excellent yield and selectivity were achieved in methanol under the same conditions (> 99%, Table S1, entry 7). Not surprisingly, an enhancing rate of **2a**/**1a** can result in an increasing reaction rate (Table S1, entries 7–10). When the mole ratio of both substrates is 10, however, the model reaction possesses the highest selectivity and quantitative yield (Table S1, entry 7). In addition, an inferior photocatalytic yield and selectivity were shown under green or white light irradiation (Table S1, entries 11 and 12). The **1a** was uncomfortably converted into the product **3a** in nitrogen gas, indicating the important role of oxygen in the photocatalytic process (Table S1, entry 13). The control experiments revealed that the light, and photocatalyst are essential for this reaction (Table S1, entries 14 and 15). Under the optimized conditions, the DA-CMP2 and DA-CMP1 as the photocatalyst achieved excellent conversions with a low selectivity (Table S1, entries 16 and 17), which implying the importance of DA-CMP structure.

In order to further research the influence of the different structure on photocatalytic performances, a series of control experiments were carried out. Under visible-light irradiation and using oxygen as an oxidation, **1a** can be transformed into hemiaminal **4** in methanol by DA-CMP2 and DA-CMP3, respectively (Fig. 3a). After 25 minutes, 97% conversion of **1a** was achieved using DA-CMP3 as a heterogeneous photocatalyst. In contrast, when DA-CMP2 was used as a photoinitiator, the conversion reaction of **1a** has a faster conversion rate under the same conditions, and nearly completely conversion of **1a** was realized within 10 minutes. This may be attributed to DA-CMP2 having better
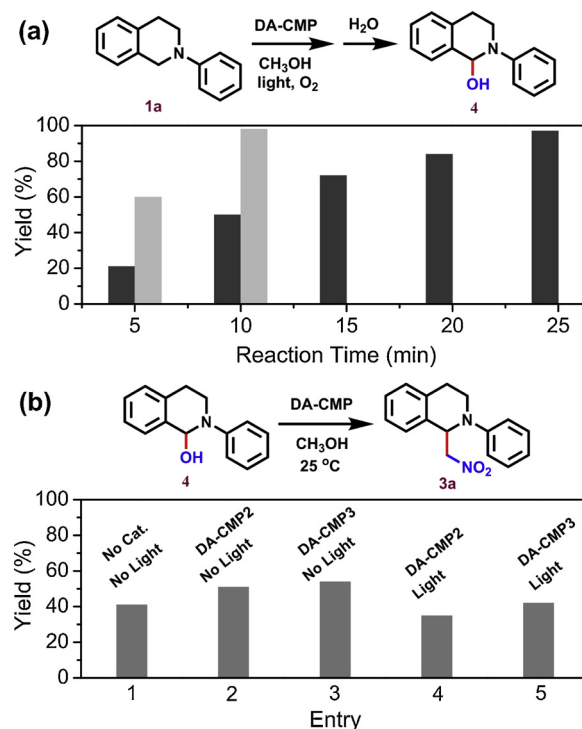
Fig. 3. (a) The photocatalytic synthesis of 4 using DA-CMP2 (gray column) and DA-CMP3 (black column) as the photocatalyst. Reaction conditions: DA-CMP (2.0 mg), 1a (0.1 mmol), dry methanol (1.0 mL), O_2 (1.0 bar), 30 W blue LED lamp with 460 nm, 25 °C. (b) The conversion of the intermediate 4 into 3a. Reaction conditions: DA-CMP (2.0 mg), 4 (0.1 mmol), 2a (1.0 mmol), methanol (1.0 mL), O_2 (1.0 bar), 30 W blue LED lamp with 460 nm, 25 °C, 7.0 min (For interpretation of the references to colour in this figure legend, the reader is referred to the web version of this article).
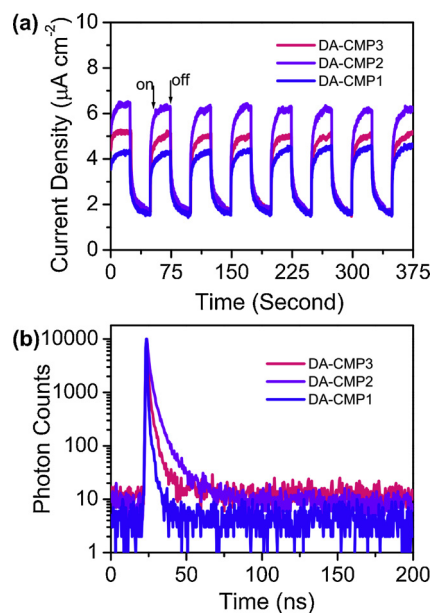
Fig. 4. (a) Transient photocurrent response of DA-CMPs under visible-light irradiation. (b) Photoluminescence decay traces of DA-CMPs.

photocatalytic activity than the DA-CMP3. Indeed, the DA-CMPs display a transient photocurrent response to visible light, which shows the generation, separation and migration of photoinduced charge carriers in the photocatalysts. Fig. 4a shows the transient photocurrent intensities of DA-CMPs with several repeating cycles of intermittent on-

off irradiation. It is clear that the DA-CMP2 exhibited a more powerful photocurrent under light irradiation compared to DA-CMP3 and DA-CMP1, which could be attributed to the more effective separation of the photoinduced electron-hole pairs and faster interfacial charge transport. Furthermore, the photoluminescent emission intensity of DA-CMP2 was much lower than that of other DA-CMPs, indicating that the recombination of the electron-hole pairs is largely hindered for DA-CMP2 (Fig. S7). In addition, the lifetimes of the carriers for DA-CMPs were determined by the fluorescence decay profiles. As shown in Fig. 4b, DA-CMP2 shows a lifetime of 3.35 ns, while the shorter fluorescence lifetime for DA-CMP3 (1.38 ns) and DA-CMP1 (0.75 ns) was obtained. The prolonged lifetime for charge carriers means enhanced reactivity, which is in accordance with results of the photocatalytic experiments (Fig. 3a).

On the other hand, the coupling reaction of hemiaminal 4 with 2a is still studied in detail (Fig. 3b). The result of control experiments indicates that light and catalyst are not necessary for this reaction (Fig. 3b, entry 1, yield of 42%). In the presence of porous polymers, however, the reaction shows a faster conversion rate and the target compound 3 was obtained with yield of 51% for DA-CMP2 and 54% for DA-CMP3, respectively (Fig. 3b, entries 2 and 3), that indicated DA-CMP3 has a stronger promoting effect for the coupling reaction than that of DA-CMP2. Under both light and polymer, two CMPs also display a similar effect (Fig. 3b, entries 4 and 5). Therefore, in the context, we can think that the CDC model reaction of 1a with nitromethane 2a consists of two steps. Although DA-CMP2 is more beneficial to the first step involving the photocatalysis process, it is unfavorable to the second step reaction compared with DA-CMP3. Overall consideration for two steps, the CDC model reaction over DA-CMP3 has a faster conversion rate into 3a.

It is well known that active oxygen species like single oxygen $^1O_2$ and superoxide radical anion $O_2^{\cdot-}$ were found to play a key role in aerobic reaction photosensitized by macromolecular photosensitizers [61–64]. To evaluate the generation ability of active oxygen species in the photocatalytic DA-CMP systems, therefore, 5,5-dimethyl-1-pyrroline-N-oxide (DMPO) and 2,2,6,6-tetramethylpiperiding (TEMP) were used as superoxide radical anion $O_2^{\cdot-}$ and singlet oxygen $^1O_2$ scavengers in the electron spin resonance (ESR) measurements. As shown in Fig. 5a, the typical characteristic of $O_2^{\cdot-}$ was trapped upon irradiation of the air-saturated CH_3CN mixture of DA-CMP2 or DA-CMP3, TEMP and 1a. However, when DMPO was used instead of TEMP in the same air-saturated solution, the nitroxide radical TEMPO was hardly detected, while in the absence of 1a the signal was easily observed (Fig. 5b). These findings indicate that the effective electron transfer between excited DA-CMP and 1a can be importantly suppressed the production of $^1O_2$ [65,66].

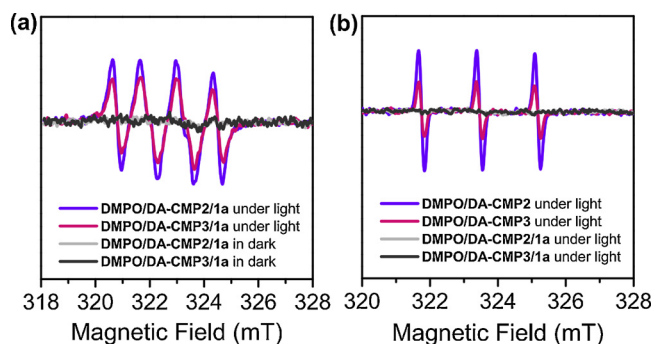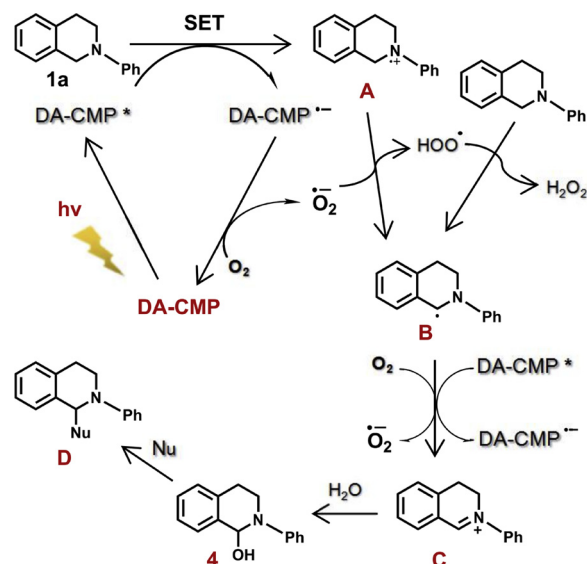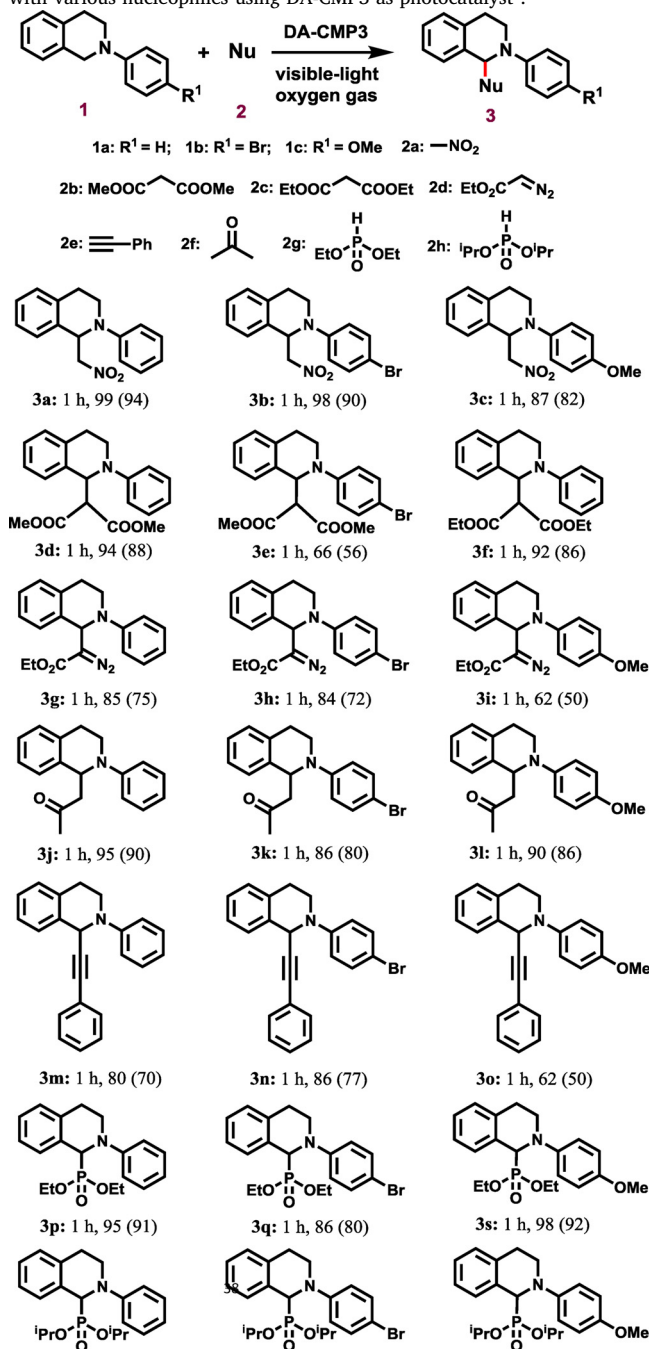**Fig. 6.** Proposed reaction pathways for the aerobic photocatalytic C–H functionalizations by DA-CMP.

Based on the current results and literature reports [61–66] a plausible reaction mechanism for the photocatalytic CDC reaction by DA-CMP is proposed as shown in Fig. 6. Upon irradiation of visible-light, the DA-CMP generates the excited species DA-CMP*, that is reductively quenched by the substrate 1a via a single electron transfer (SET) process to form an radical cation A and radical anion DA-CMP$^{\cdot-}$. The generated radical anion DA-CMP$^{\cdot-}$ is subsequently quenched by molecular O_2 to form the superoxide anion $O_2^{\cdot-}$ and simultaneously to regenerate DA-CMP. The superoxide anion $O_2^{\cdot-}$ subsequently abstracts a proton from A to produce the hydroperoxide radical HOO$^\cdot$ and the intermediate B. Then, the obtained hydroperoxide radical HOO$^\cdot$ abstract a hydrogen atom form the substrate1a to afford the B alone with the formation of H_2O_2. The B lose one electron to give the iminium ion C. And then the intermediate C reacts with the water in the system to get the hemiaminal 4 [67,68]. Finally, the compound 4 undergoes nucliophilic addition to provide the desired product D.

To investigate the general feasibility of new polymer skeleton as an efficient photocatalyst, we then screened the substrate scope for aerobic CDC reaction. As summarized in Table 1, a series of substituted 1,2,3,4-tetrahydroisoquinoline derivatives 1a-c with nitromethane were able to subject to the aza-Henry reaction, thus resulting in the desired reaction compounds 3a-c in good to excellent yields. The electronic characterizations of the substituent group in the diffrent substrates had little effect on the yields. Next, we investigated the applicability of other types of nucleophilic reagents. Under visible-light irradiation, dialkyl malonates were treated smoothly with 1a to afford the products 3d and 3f in excellent yields. While 1b with an electron-withdrawing group in the phenyl group gave a moderate yield for 3e. Further, a series of aerobic CDC reaction of 1 with ethyl diazoacetate were conducted. The good catalytic yields were shown in Table 1(entries 3g-i). Subsequently, using acetone as nucleophile, we researched the dehydrogenative-Mannich reactions combining the photocatalytic oxidation and proline-organocatalysis, which provides a very powerful method to valuable β-amino-ketones. In the presence of proline, an enamine with increased nucleophilicity can be formed in situ, and the Mannich reaction proceeded smoothly by DA-CMP3 to give the Mannich-type products 3j-l in good yield. Currently, coupled photocatalysis and metal-mediated coupling reactions are a fascinating strategy for organic synthesis. In order to explore the applications of new framework materials in organic synthesis reactions in depth, DA-CMP3 was performed as photocatalyst for the coupled visible-light mediated oxidation and the Cu(I)-assisted alkynylation. It is found that new polymer can drive the coupled dual-

Fig. 5. (a) ESR spectra of the mixture DA-CMP (1.0 mg mL⁻¹), 1a (1.0 × 10⁻² M) and DMPO (0.1 M) in air-saturated CH_3CN in dark and upon light irradiation. (b) ESR spectra of the mixture DA-CMP (1.0 mg mL⁻¹) and TEMP (0.1 M) in air-saturated CH_3CN upon light irradiation; ESR spectra of the mixture DA-CMP (1.0 mg mL⁻¹), 1a (1.0 × 10⁻² M) and TEMP (0.1 M) in air-saturated CH_3CN upon light irradiation.

Table 1

Photocatalytic C–C/C–P coupling reaction of N-phenyltetrahydroisoquinonlines with various nucleophiles using DA-CMP3 as photocatalyst[a].

1a: R[1] = H;   1b: R[1] = Br;   1c: R[1] = OMe   2a: —NO₂

2b: MeOOC—COOMe   2c: EtOOC—COOEt   2d: EtO₂C—N₂

2e: ≡—Ph   2f: (acetone)   2g: EtO-P(=O)(H)-OEt   2h: iPrO-P(=O)(H)-OiPr

3a: 1 h, 99 (94)

3b: 1 h, 98 (90)

3c: 1 h, 87 (82)

3d: 1 h, 94 (88)

3e: 1 h, 66 (56)

3f: 1 h, 92 (86)

3g: 1 h, 85 (75)

3h: 1 h, 84 (72)

3i: 1 h, 62 (50)

3j: 1 h, 95 (90)

3k: 1 h, 86 (80)

3l: 1 h, 90 (86)

3m: 1 h, 80 (70)

3n: 1 h, 86 (77)

3o: 1 h, 62 (50)

3p: 1 h, 95 (91)

3q: 1 h, 86 (80)

3s: 1 h, 98 (92)

[a]Reaction conditions: DA-CMP3 (2.0 mg), 1 (0.1 mmol), 2 (1.0 mmol), methanol (1.0 mL), O₂ (1.0 bar), 30 W blue LED lamp with 460 nm, 25 °C, 1.0 h. The yields detected by NMR spectroscopy and the isolated product yields are given in parentheses.

catalytic process smoothly, and the propargyl amines **3m-o** were afforded in good yield.

The α-amino phosphonate and α-amino phosphonic acid compounds have been widely investigated in medicinal chemistry owing to their antibacterial activities [69,70]. Therefore, the success of C–C formation by DA-CMP3 inspired us to explore C–P bond formation reactions. To our delight, a variety of tertiary amines **1a-c** also react smoothly with phosphine oxides in the presence of DA-CMP3 under the optimized conditions. The good to excellent yields of cross-coupling products, specifically α-amino dialkyl phosphonates **3p-v**, were obtained
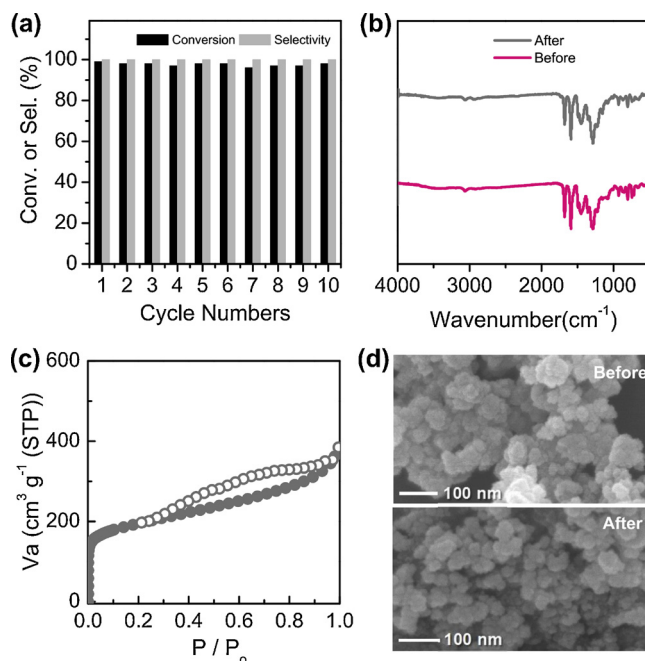

Fig. 7. (a) Recycling catalytic experiment of DA-CMP3 for the model reaction under visible-light irradiation: 25 °C, O₂ (1.0 bar), 30 W blue LED lamp with 460 nm. (b) FT-IR spectra of DA-CMP3 before and after ten runs. (c) Nitrogen adsorption (full) and desorption (empty) isotherm of DA-CMP3 after ten runs. (d) SEM images of DA-CMP3 before and after ten runs (For interpretation of the references to colour in this figure legend, the reader is referred to the web version of this article).

regardless of the electronic property in substrates and the steric effect of nucleophile.

To further explore the recovery and reusing of DA-CMP3 as a solid photocatalyst in carbon-hydrogen functionalization under visible light irradiation, the model reaction of **1a** and **2a** was selected for the research. In each cycle, the photocatalyst DA-CMP3 was easily isolated from the reaction mixtures by centrifugation, and then washed, dried and utilized in the next run of the model reaction. It was found the DA-CMP3 can efficiently recycled and reused at least ten cycles without obvious loss of photocatlytic activity and selectivity (Fig. 7a). Pleasurably, the polymer framework after reusing still retained the original skeleton connectivity (Fig. 7b), aggregated morphology (Fig. 7d) and high specific surface area (713 m² g⁻¹, Fig. 7c). This can be attributed to the excellent stability of the material. In addition, we still assessed the possibility of the large scale preparetion using **1a** (0.53 g, 2.5 mmol) as a reactant. As shown in Scheme S1, a high yield (92%) was obtained in the scaled-up synthetic process. The outstanding properties of DA-CMP including high photocatalytic activity, wide substrate adaptability, good recyclability and stability make it ideal platform for commercial application.

The possible application of the new network photocatalyst in industry was still demonstrated through an easy-to-build continuous flow reactor (Fig. S10). The DA-CMP3 monolith (5.0 mg) was placed in a photoreactor that contains fluorinated ethylene propylene (FEP) tube and a glass column (r = 0.35 cm, L = 5.0 cm). The mixture solution of **1a/2a** was mixed with O₂ (5.0 mL min⁻¹) by a syringe pump and pumped through the microreactor with the desired flow rate (150.0 μL min⁻¹) under visible-light irridiation (Fig. S11). Full conversion to the target product **3a** was obtained after 0.75 h.

4. Conclusions

In summary, we have demostrated that the construction of CMPs through oxidative coupling of single carbazole based DA monomers is

an effective strategy for sieving the excellent photocatalyst. Based on the different carbazole based DA derivatives, three DA-CMPs have been successfully designed and constructed, and their color, porosity and photoelectric properties including adsorption, emission, lifetime, optical bandgaps and energy levels and transient photocurrent response as well as photocatalytic activity were conveniently tuned by selecting different DA monomer with tunable electron-deficient moiety. Based on the results of the control experiments, DA-CMP2 possesses the best photocatalytic activity in three polymer materials, due to more effective separation of the photoinduced electron-hole pairs, faster interfacial charge transport and stronger generation ability of active oxygen species. Combining the permanent porosity, outstanding stability and optoelectronic properties, the DA-CMPs were found to be excellent heterogeneous photocatalysts for the oxidative C–H functionalizations of N-aryltetradroisoquinolines with great catalytic activity, extensive substrate adaptability and outstanding reusability under visible-light irradiation and molecular oxygen. A mechanism research was performed to indicate the important roles of the photogenerated electron-hole pairs and active oxygen species during the catalytic cycle. We also highlight that the oxidative coupling of single photoactive DA monomers is a straightforward approach to screen other porous organic polymers based photocatalysts for a wider range of organic transformations.

Acknowledgment

Appendix A. Supplementary data

Supplementary material related to this article can be found, in the online version, at doi:https://doi.org/10.1016/j.apcatb.2018.11.032.

References

[1] D.A. Nicewicz, D.W.C. MacMillan, Merging photoredox catalysis with organocatalysis: the direct asymmetric alkylation of aldehydes, Science 322 (2008) 77–80.
[2] K. Zeitler, Photoredox catalysis with visible light, Angew. Chem., Int. Ed. 48 (2009) 9785–9789.
[3] D. Spasiano, R. Marotta, S. Malato, P. Fernandez-Ibanez, I. Somma, Solar photocatalysis: materials, reactors, some commercial, and pre-industrialized applications. A comprehensive approach, Appl. Catal. B: Environ. 170-171 (2015) 90–123.
[4] D. Schultz, T.P. Yoon, Solar synthesis: prospects in visible light photocatalysis, Science 343 (2014) 1239176.
[5] J.M. Narayanam, C.R. Stephenson, Visible light photoredox catalysis: applications in organic synthesis, Chem. Soc. Rev. 40 (2011) 102–113.
[6] M. Rueping, C. Vila, A. Szadkowska, R.M. Koenigs, J. Fronert, Photoredox catalysis as an efficient tool for the aerobic oxidation of amines and alcohols: bioinspired demethylations and condensations, ACS Catal. 2 (2012) 2810–2815.
[7] J. Xuan, W. Xiao, Visible-light photoredox catalysis, Angew. Chem. Int. Ed. 51 (2012) 6828–6838.
[8] Z. Hao, S. Li, J. Sun, S. Li, F. Zhang, Efficient visible-light-driven depolymerization of oxidized lignin to aromatics catalyzed by an iridium complex immobilized on mesocellular silica foams, Appl. Catal. B: Environ. 237 (2018) 366–372.
[9] D.P. Hari, B. König, The photocatalyzed meerwein arylation: classic reaction of aryl diazonium salts in a new light, Angew. Chem., Int. Ed. 52 (2013) 4734–4743.
[10] M. Hopkinson, B. Sahoo, J. Li, F. Glorius, Dual catalysis sees the light: combining photoredox with organo-, acid, and transition-metal catalysis, Chem. Eur. J. 20 (2014) 3874–3886.
[11] T. Yoon, M. AIschay, J. Du, Visible light photocatalysis as a greener approach to photochemical synthesis, Nat. Chem. 2 (2010) 527–532.
[12] L. Shi, W. Xiao, Photoredox functionalization of C–H bonds adjacent to a nitrogen atom, Chem. Soc. Rev. 41 (2012) 7687–7697.
[13] R. Li, J. Byun, W. Huang, C. Ayel, L. Wang, K.A.I. Zhang, Poly(benzothiadiazoles) and their derivatives as heterogeneous photocatalysts for visible-light-driven chemical transformations, ACS Catal. 8 (2018) 4735–4750.
[14] D. Masih, Y. Ma, S. Rohani, Graphitic C_3N_4 based noble-metal-free photocatalyst systems: a review, Appl. Catal. B: Environ. 206 (2017) 556–588.
[15] X. Wang, S. Blechert, M. Antoniettiok, Polymeric graphitic carbon nitride for heterogeneous photocatalysis, ACS Catal. 2 (2012) 1596–1606.
[16] T. Zhang, W. Lin, Metal-organic frameworks for artificial photosynthesis and photochemistry, Chem. Soc. Rev. 43 (2014) 5982–5993.
[17] X. Deng, Z. Li, H. García, Visible light induced organic transformations using metal-organic-frameworks (MOFs), Chem. Eur. J. 23 (2017) 11189–11209.
[18] Y. Tian, W. Li, C. Zhao, Y. Wang, B. Zhang, Q. Zhang, Fabrication of hollow mesoporous SiO_2-BiOCl@PANI@Pd photocatalysts to improve the photocatalytic performance under visible light, Appl. Catal. B: Environ. 213 (2017) 136–146.
[19] L. Chen, J. Tang, L.N. Song, P. Chen, J. He, C.T. Au, S.F. Yin, Heterogeneous photocatalysis for selective oxidation of alcohols and hydrocarbons, Appl. Catal. B: Environ. 242 (2019) 379–388.
[20] X. Wang, K. Maeda, A. Thomas, K. Takanabe, G. Xin, M. Carlsson, K. Domen, M. Antonietti, A metal-free polymeric photocatalyst for hydrogen production from water under visible light, Nat. Mater. 8 (2009) 76–80.
[21] A.I. Cooper, Conjugated microporous polymers, Adv. Mater. 21 (2009) 1291–1295.
[22] Y. Xu, S. Jin, H. Xu, A. Nagai, D. Jiang, Conjugated microporous polymers: design, synthesis and application, Chem. Soc. Rev. 42 (2013) 8012–8031.
[23] A. Thomas, Functional materials: from hard to Soft Porous frameworks, Angew. Chem. Int. Ed. 49 (2010) 8328–8344.
[24] R.S. Sprick, J. Jiang, B. Bonillo, S. Ren, S.T. Ratvijitvech, P. Guiglion, M.A. Zwijnenburg, D.J. Adams, A.I. Cooper, Tunable organic photocatalysts for visible-light-driven hydrogen evolution, J. Am. Chem. Soc. 137 (2015) 3265–3270.
[25] S. Kuecken, A. Acharjya, L. Zhi, M. Schwarze, R. Schomacker, A. Thomas, Fast tuning of covalent triazine frameworks for photocatalytic hydrogen evolution, Chem. Commun. 53 (2017) 5854–5857.
[26] S. Bi, Z. Lan, S. Paasch, W. Zhang, Y. He, C. Zhang, F. Liu, D. Wu, X. Zhuang, E. Brunner, X. Wang, F. Zhang, Substantial cyano-substituted fully sp^2-carbon-linked framework: metal-free approach and visible-light-driven hydrogen evolution, Adv. Funct. Mater. 27 (2017) 1703146.
[27] Y. Xu, N. Mao, C. Zhang, X. Wang, J. Zeng, Y. Chen, F. Wang, J. Jiang, Appl. Rational design of Donor-π-Acceptor conjugated microporous polymers for photocatalytic hydrogen production, Appl. Catal. B: Environ. 228 (2018) 1–9.
[28] I. Nath, J. Chakraborty, P. Heynderickx, F. Verpoort, Engineered synthesis of hierarchical porous organic polymers for visible light and natural sunlight induced rapid degradation of azo, thiazine and fluorescein based dyes in a unique mechanistic pathway, Appl. Catal. B: Environ. 227 (2018) 102–113.
[29] M. Liras, M. Lglesias, F. Sánchez, conjugated microporous polymers incorporating bodipy moieties as light-emitting materials and recyclable visible-light photocatalysts, Macromolecules 49 (2016) 1666–1673.
[30] C. Su, R. Tandiana, B. Tian, A. Sengupta, W. Tang, J. Su, K.P. Loh, Visible-light photocatalysis of aerobic oxidation reactions using carbazolic conjugated microporous polymers, ACS Catal. 6 (2016) 3594–3599.
[31] H. Liang, Q. Chen, B. Han, Cationic polycarbazole networks as visible-light heterogeneous photocatalysts for oxidative organic transformations, ACS Catal. 8 (2018) 5313–5322.
[32] X. Ding, B. Han, Metallophthalocyanine-based conjugated microporous polymers as highly efficient photosensitizers for singlet oxygen generation, Angew. Chem. Int. Ed. 54 (2015) 6536–6539.
[33] K. Zhang, D. Kopetzki, P. Seeberger, M. Antonietti, F. Vilela, Surface area control and photocatalytic activity of conjugated microporous poly(benzothiadiazole) networks, Angew. Chem., Int. Ed. 52 (2013) 1432–1436.
[34] X. Chen, M. Addicoat, E. Jin, L. Zhai, H. Xu, N. Huang, Z. Guo, L. Liu, S. Irle, D. Jiang, Locking covalent organic frameworks with hydrogen bonds: general and remarkable effects on crystalline structure, physical properties, and photochemical activity, J. Am. Chem. Soc. 137 (2015) 3241–3247.
[35] Z. Wang, S. Ghasimi, K. Landfester, K.A.I. Zhang, Molecular structural design of conjugated microporous poly(benzooxadiazole) networks for enhanced photocatalytic activity with visible light, Adv. Mater. 27 (2015) 6265–6270.
[36] J. Ko, N. Kang, N. Park, H. Shin, S. Kang, S. Lee, H. Kim, T. Ahn, S. Son, Hollow microporous organic networks bearing triphenylamines and anthraquinones: diffusion pathway effect in visible light-driven oxidative coupling of benzylamines, ACS Macro Lett. 4 (2015) 669–672.
[37] J. Luo, X. Zhang, J. Zhang, Carbazolic porous organic framework as an efficient, metal-free visible-light photocatalyst for organic synthesis, ACS Catal. 5 (2015) 2250–2254.
[38] Y. Li, M. Liu, L. Chen, Polyoxometalate built-in conjugated microporous polymers for visible-light heterogeneous photocatalysis, J. Mater. Chem. A Mater. Energy Sustain. 5 (2017) 13757–13762.
[39] S. Bhunia, S. Das, R. Jana, S. Peter, S. Bhattacharya, M. Addicoat, A. Bhaumik, Anirban Pradhan, Electrochemical stimuli-driven facile metal-free hydrogen evolution from pyrene-porphyrin-based crystalline covalent organic framework, ACS Appl. Mater. Inter. 9 (2017) 23843–23851.
[40] W. He, C. Wu, Incorporation of Fe-phthalocyanines into a porous organic framework for highly efficient photocatalytic oxidation of arylalkanes, App. Catal. B: Environ. 234 (2018) 290–295.
[41] H.J. Hou, X.H. Zhang, D.K. Huang, X. Ding, S.Y. Wang, X.L. Yang, S.Q. Li, Y.G. Xiang, H. Chen, Conjugated microporous poly(benzothiadiazole)/TiO_2 heterojunction for visible-light-driven h_2 production and pollutant removal, Appl. Catal. B: Environ. 203 (2017) 563–571.
[42] X. Yang, Y. Xiang, Y. Qu, X. Ding, H. Chen, Novel in situ fabrication of conjugated microporous poly(benzothiadiazole)-bi₂moo₆ z-scheme heterojunction with enhanced visible light photocatalytic activity, J. Catal. 345 (2017) 319–328.
[43] Y. Xiang, X. Zhang, X. Wang, X. Ding, D. Huang, H. Chen, Molecular structure design of conjugated microporous poly(dibenzo[b,d]thiophene5,5-dioxide) for optimized photocatalytic NO removal, J. Catal. 357 (2018) 188–194.
[44] Y. Zhi, Z. Li, X. Feng, H. Xia, Y. Zhang, Z. Shi, Y. Mu, X. Liu, Covalent organic frameworks as metal-free heterogeneous photocatalysts for organic transformations, J. Mater. Chem. A Mater. Energy Sustain. 5 (2017) 22933–22938.
[45] J. Li, A. Grimsdale, Carbazole-based polymers for organic photovoltaic devices, Chem. Soc. Rev. 39 (2010) 2399–2410.
[46] P. Boudreault, S. Beaupré, M. Leclerc, Polycarbazoles for plastic electronics, Polym.

Chem. 1 (2010) 127–136.

[47] Q. Chen, M. Luo, P. Hammershoj, D. Zhou, Y. Han, B. Laursen, C. Yan, B. Han, Microporous polycarbazole with high specific surface area for gas storage and separation, J. Am. Chem. Soc. 134 (2012) 6084–6087.

[48] Y. Zhang, S.A.Y. Zou, X. Luo, Z. Li, H. Xia, X. Liu, Y. Mu, Gas uptake, molecular sensing and organocatalytic performances of a multifunctional carbazole-based conjugated microporous polymer, J. Mater. Chem. A Mater. Energy Sustain. 2 (2014) 13422–13430.

[49] A. Palma-Cando, D. Preis, U. Scherf, Silicon- or carbon-cored multifunctional carbazolyl monomers for the electrochemical generation of microporous polymer film, Macromolecules 49 (2016) 8041–8047.

[50] J. Luo, X. Zhang, J. Lu, J. Zhang, fine tuning the redox potentials of carbazolic porous organic frameworks for visible-light photoredox catalytic degradation of lignin*β*-O4 models, ACS Catal. 7 (2017) 5062–5070.

[51] Q. Chen, B. Han, Microporous polycarbazole materials: from preparation and properties to applications, Macromol. Rapid Commun. 39 (2018) 1800040.

[52] S. Qiao, W. Huang, H. Wei, T. Wang, R. Yang, Fine tailoring the steric configuration of initial building blocks to construct ultramicroporous polycarbazole networks with high CO$_2$ uptake and selectivity of CO$_2$ Over N$_2$, Polymer 70 (2015) 52–58.

[53] A. Palmacando, U. Scherf, Electrogenerated thin films of microporous polymer networks with remarkably increased electrochemical response to nitroaromatic analytes, ACS Appl. Mater. Interfaces 7 (2015) 11127–11133.

[54] J. Liu, J.L. Meng, W. Zhu, C. Zhang, H. Zhang, Y. Yao, Z. Wang, P. He, X. Zhang, Y. Wang, Y. Zhen, H. Dong, Y. Yi, W. Hu, A cross-dipole stacking molecule of an anthracene derivative: integrating optical and electrical properties, J. Mater. Chem. C Mater. Opt. Electron. Devices 3 (2015) 3068–3071.

[55] D. Freeman, L. Furst, A. Condie, Allison C. Stephenson, Functionally diverse nucleophilic trapping of iminium intermediates generated utilizing visible light org, Lett. 14 (2012) 94–97.

[56] R. Li, Z. Wang, L. Wang, B. Ma, S. Ghasimi, H. Lu, K. Landfester, K.A.I. Zhang, Photocatalytic selective bromination of electron-rich aromatic compounds using microporous organic polymers with visible light, ACS Catal. 6 (2016) 1113–1121.

[57] Q. Sun, Z. Dai, X. Meng, F.S. Xiao, Porous polymer catalysts with hierarchical structures, Chem. Soc. Rev. 44 (2015) 6018–6034.

[58] C. Li, Cross-dehydrogenative coupling (CDC): exploring C−C bond formations beyond functional group transformations, Acc. Chem. Res. 42 (2009) 335–344.

[59] S. Murahashi, D. Zhang, Ruthenium catalyzed biomimetic oxidation in organic synthesis inspired by cytochrome P-450, Chem. Soc. Rev. 37 (2008) 1490–1501.

[60] Z. Li, Y. Pi, D. Xu, Y. Li, W. Peng, G. Zhang, F. Zhang, X. Fan, Utilization of MoS$_2$ and graphene to enhance the photocatalytic activity of Cu$_2$O for oxidative C−C bond formation, Appl. Catal. B: Environ. 213 (2017) 1–8.

[61] N. Kang, J. Park, J. Chun, E. Kim, H. Shim, S. Lee, H. Kim, T. Ahn, J. Lee, S. Son, tandem synthesis of photoactive benzodifuran moieties in the formation of microporous organic networks, Angew. Chem., Int. Ed. 52 (2013) 6228–6232.

[62] H. Bartling, A. Eisenhofer, B. König, R. Gschwind, The Photocatalyzed Aza-henry reaction of N-aryltetrahydroisoquinolines: comprehensive mechanism, H$^{\cdot-}$ versus H$^{+\cdot}$ abstraction, and background reactions, J. Am. Chem. Soc. 138 (2016) 11860–11871.

[63] Y. Zhi, K. Li, H. Xia, M. Xue, Y. Mu, X. Liu, Robust porous organic polymers as efficient heterogeneous organo-photocatalysts for aerobic oxidation reactions, J. Mater. Chem. A Mater. Energy Sustain. 5 (2017) 8697–8704.

[64] Z. Li, Z. Zhou, J. Ma, Y. Li, W. Peng, G. Zhang, F. Zhang, X. Fan, Hierarchical photocatalyst of In$_2$S$_3$ on exfoliated MoS$_2$ nanosheets for enhanced visible-light-driven Aza-henry reaction, Appl. Catal. B: Environ. 237 (2018) 288–294.

[65] Q. Liu, Y. Li, H. Zhang, L. Wu, Reactivity and mechanistic insight into visible-light-induced aerobic cross dehydrogenative coupling reaction by organophotocatalysts, Chem. Eur. J. 18 (2012) 620–627.

[66] W. Zhang, Q. Li, Q. Zhang, Y. Lu, H. Lu, W. Wang, X. Zhao, X. Wang, Robust metal-organic framework containing benzoselenadiazole for highly efficient aerobic cross-dehydrogenative coupling reactions under visible light, Inorg. Chem. 55 (2016) 1005–1007.

[67] A. Condie, C. Stephenson, Visible-light photoredox catalysis: Aza-Henry reactions via C-H functionalization, J. Am. Chem. Soc. 132 (2010) 1464–1465.

[68] G. Zhao, C. Yang, L. Guo, H. Sun, C. Chen, W. Xia, visible light-induced oxidative coupling reaction: easy access to mannich-type products, Chem. Commun. 48 (2012) 2337–2339.

[69] X. Wang, Q. Meng, J. Zhong, X. Gao, T. Lei, L. Zhao, Z. Li, B. Chen, C. Tung, L. Wu, The singlet excited state of BODIPY promoted aerobic cross-dehydrogenative-coupling reactions under visible light, Chem. Commun. 51 (2015) 11256–11259.

[70] W. To, Y. Liu, T. Lau, C. Che, A robust palladium (II)–porphyrin complex as catalyst for visible light induced oxidative C-H functionalization, Chem. Eur. J. 19 (2013) 5654–5664.